

Scenario Liquefaction Hazard Maps of Santa Clara Valley, Northern California

by Thomas L. Holzer, Thomas E. Noce, and Michael J. Bennett

Abstract Maps showing the probability of surface manifestations of liquefaction in the northern Santa Clara Valley were prepared with liquefaction probability curves. These curves were based on complementary cumulative frequency distributions of the liquefaction potential index (LPI) for surficial geologic units in the study area. LPI values were computed with extensive cone penetration test soundings. Maps were developed for three earthquake scenarios, an **M** 7.8 event on the San Andreas fault comparable to the 1906 event, an **M** 6.7 event on the Hayward fault comparable to the 1868 event, and an **M** 6.9 event on the Calaveras fault. Ground motions were estimated with the Boore and Atkinson (2008) attenuation relation. Liquefaction is predicted for all three events in young Holocene levee deposits along the major creeks. Liquefaction probabilities are highest for the **M** 7.8 earthquake, ranging from 0.33 to 0.37 if a 1.5 m deep water table is assumed, and from 0.10 to 0.14, if a 5 m deep water table is assumed. Liquefaction probabilities of the other surficial geologic units are less than 0.05. Probabilities for the scenario earthquakes are generally consistent with observations during historical earthquakes.

Introduction

Regional mapping of liquefaction hazard has evolved during the last few decades from research to regulatory endeavors. Despite this evolution, most liquefaction hazard mapping remains descriptive and qualitative in nature. This descriptive state-of-the-art of mapping liquefaction hazard stands in contrast with the quantitative state-of-the-art of mapping earthquake shaking hazard. Probabilistic mapping of shaking, which was originally proposed by Cornell (1968), is now firmly established and is widely used in engineering practice (McGuire, 2004). In fact, confidence in the methodology has progressed to where it is now the basis in many building codes for estimating shaking hazard (e.g., Building Seismic Safety Council [BSSC], 2001). The methodology is known as probabilistic seismic hazard analysis. A comparable probabilistic framework is an important need for future liquefaction hazard mapping.

The increasing implementation of regulatory seismic hazard zone maps is an important motivation for the development of probabilistic liquefaction hazard maps (California Geological Survey [CGS], 2004). Regulatory maps tend to be of a binary nature, indicating only where special studies either are or are not required. Although regulatory maps serve the useful purpose of identifying areas with a potential liquefaction hazard and prompting site specific investigations, they can be confusing to citizens engaged in real estate transactions when the liquefaction hazard is disclosed. Probabilistic maps indicate the degree of hazard within hazard

zones and thereby provide a perspective on actual risk to the user. Ultimately, it may even be possible to fully delineate and regulate these hazard zones on the basis of probabilistic criteria.

The absence of a widely accepted engineering demand parameter, that is, a liquefaction intensity parameter that measures the severity of liquefaction at a site, is a major obstacle to the implementation of a probabilistic framework for liquefaction hazard mapping. Several investigators recently have produced probabilistic liquefaction hazard maps for earthquake scenarios that use a parameter known as the liquefaction potential index (LPI) as an intensity parameter (see Holzer, 2008, table 1). In this investigation, LPI was applied to map liquefaction probabilities in the northern part of the Santa Clara Valley in the San Francisco Bay region of California (Fig. 1). Although the methodology is conceptually similar to that described by Holzer, Bennett, *et al.* (2006) for liquefaction hazard mapping of the greater Oakland area, the revised mapping procedure more readily permits the incorporation of spatially variable ground motion and different earthquake magnitudes. In the revised procedure, peak ground accelerations (PGAs) were computed for 50 m cells in the study area with a ground-motion attenuation relation for a scenario earthquake. Then, liquefaction probabilities were computed at each cell based on the PGA value and earthquake magnitude and liquefaction probability curves that were developed for the surficial geology at the cell

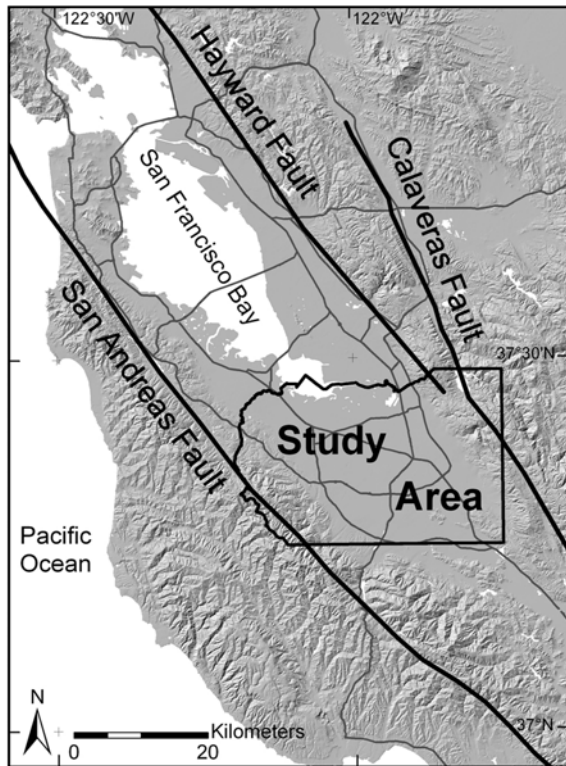


Figure 1. Location of the study area.

location. Computations were performed with ArcGIS ModelBuilder.

Engineering Geology

Surficial Geology

The Santa Clara Valley is at the southern end of the San Francisco Bay (Fig. 1). The valley is basically a trough that has been subsiding and filling with sediment during the Quaternary period. Deposition of Quaternary alluvial fan and fluvial sediments has been influenced by both tectonic subsidence and the climatic and base level changes associated with Pleistocene glaciations and sea level fluctuations. According to Wentworth and Tinsley (2005), the 400 m of Quaternary alluvial fill beneath the valley was deposited in eight sedimentary cycles. Each sequence is bounded by unconformities, which formed during low stands of sea level when climates were considerably cooler and the surface of the valley floor was subject to either erosion or nondeposition. Deposition of alluvial sediment renewed with climatic warming and drying during the transition to interglacial conditions, with most of the deposition occurring at the beginning of each cycle.

Surficial geology in the study area was most recently mapped by Witter *et al.* (2006). Their map indicates that the valley floor is blanketed by Holocene alluvial fan deposits (Fig. 2). On the basis of the subsurface exploration conducted for this investigation, these deposits have an average

thickness in the central part of the study area of ~ 9 m. Their maximum thickness is ~ 18 m. They thin outward from the axis of the valley. These Holocene sediments were deposited after the last glacial epoch and are the most recent sedimentary cycle described by Wentworth and Tinsley (2005). Pleistocene alluvial fan deposits from earlier cycles underlie these Holocene sediments and crop out along the margins of the valley.

The surficial geology shown in Figure 2 is simplified from the mapping by Witter *et al.* (2006) to emphasize the major units that were considered in the liquefaction hazard mapping. The map also shows locations of cone penetration test (CPT) soundings that were used to characterize the liquefaction hazard. Penetration data for these soundings are available at the U.S. Geological Survey (USGS) Earthquake Program Web site (see Data and Resources section). Witter *et al.* (2006) identified three major Holocene fan facies or units: Qhfy, a coarser grained facies around the margin of the valley associated with the heads of the alluvial fans; Qhff, a finer grained facies that is the distal end of the fans; and Qhly/Qhl, levee deposits along modern creeks. The areas mapped as levee deposits presumably also include buried older Holocene channel and point bar deposits. In addition, Witter *et al.* (2006) mapped a large area around the margin of the San Francisco Bay that is underlain by estuarine deposits, Qhbm. This area was not explored for hazard mapping purposes because it was mostly inaccessible to the CPT truck that was used for the subsurface exploration. Urban development is modest in this area. The simplified map in Figure 2 also does not distinguish among Pleistocene alluvial fan deposits mapped by Witter *et al.* (2006). These deposits are identified here simply as Qpf.

The original surficial geologic map identified 18 Holocene surficial units, including many on the valley floor that were of limited extent (Witter *et al.*, 2006). It was not practical to explore systematically these minor units with the CPT because of site access limitations. To make the liquefaction hazard map, the minor units were grouped with the major unit with which we anticipated they would have the greatest similarity based on the geologic descriptions by Witter *et al.* (2006). The impact on the appearance of the resulting hazard map is modest.

Earthquake Potential

The Santa Clara Valley is bounded by two active strike-slip fault systems that are the principal components of the transform boundary between the Pacific and North American tectonic plates in the Bay area (Fig. 1). The San Andreas fault lies to the west of the study area. It generated the 1906 M 7.8 San Francisco earthquake, which ruptured 470 km of the fault. An earthquake like the 1906 event is the largest earthquake that is expected to shake the study area (Working Group on California Earthquake Probabilities [WGCEP], 2003). The Hayward and Calaveras faults lie to the east. The largest historical earthquake on these faults was the 1868

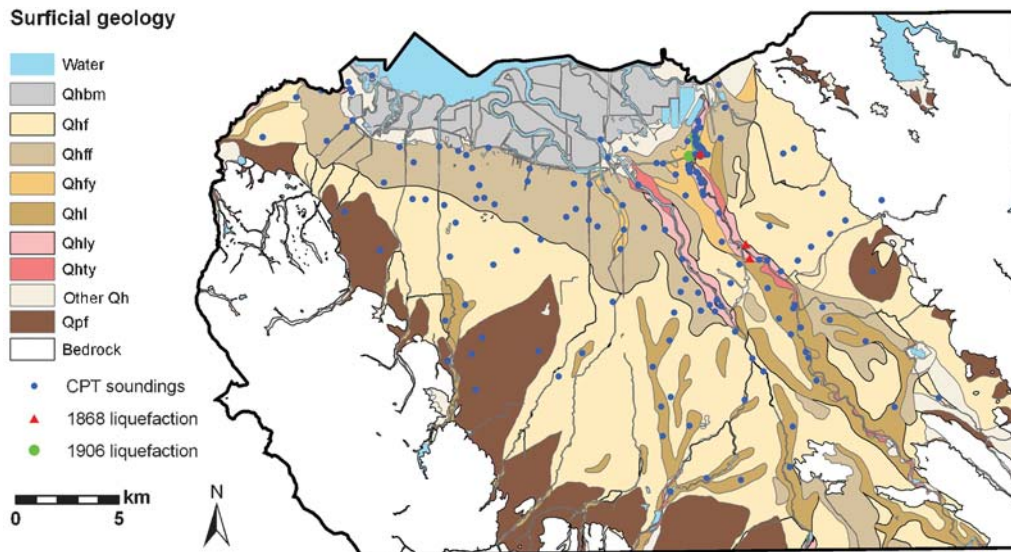


Figure 2. Surficial geology of study area, northern Santa Clara Valley, simplified from Witter *et al.* (2006) with locations of CPT soundings and liquefaction reported in 1868 and 1906. The two major accumulations of Qhly are associated with Coyote Creek (east) and Guadalupe Creek (west).

M ~6.7 Hayward earthquake. Both the 1868 and 1906 earthquakes caused liquefaction in the study area (Figs. 2 and 3). Reported liquefaction effects were confined to areas underlain by Qhly (Fig. 2). The only other large historical earthquake, the 1989 M 6.9 Loma Prieta earthquake that ruptured the southern segment of the 1906 San Andreas fault rupture, did not cause liquefaction in the study area (Holzer, 1998).

Three earthquake scenarios were considered in this investigation, the two historical events described previously and a Calaveras fault event. The likelihood of each of these events was evaluated by a USGS Working Group as part of an intensive investigation of potential earthquakes in the San Francisco Bay area (WGCEP, 2003). The group concluded that the 30 yr (2002–2031) probability is 0.05 for a repeat of the 1906 earthquake. The group also concluded that the 30 yr probability is 0.11 for a repeat of the 1868 Hayward

earthquake, which ruptured the southern segment of the fault. The southern segment is the closest portion of the Hayward fault to the study area. The higher probability of the earthquake on the southern segment of the Hayward fault relative to a 1906-like San Andreas fault event is attributable to its smaller magnitude and the longer period of elapsed time, which has allowed tectonic strain to accumulate. The seismic potential of the Calaveras fault is poorly known. The 1984 M 6.2 Morgan Hill earthquake is the largest historical earthquake on the fault. WGCEP (2003) estimated that a rupture of the central and northern segments of the Calaveras fault would produce an M 6.9 earthquake, but the 30 yr probability of the event is very low, 0.003. The study area is adjacent to the central segment of the Calaveras fault.

Methodology

Liquefaction Prediction

In this investigation, as in our earlier mapping efforts (Holzer, Bennett, *et al.*, 2006), LPI as defined by Iwasaki *et al.* (1978) was used to characterize the liquefaction hazard. Other definitions have been proposed, but redefining LPI can change the significance and interpretation of specific LPI values (Holzer, 2008). As proposed by Iwasaki *et al.* (1978), LPI weighs liquefaction factors of safety and thickness of potentially liquefiable layers according to depth. It assumes that the severity of liquefaction is proportional to

1. Cumulative thickness of the liquefied layers;
2. Proximity of the liquefied layers to the surface; and
3. Amount by which the liquefaction factor safety (FS) is less than 1.0, where FS is the ratio of the soil capacity to resist liquefaction to seismic demand imposed by the earthquake.



Figure 3. Photograph of sand boils along Coyote Creek in 1906 (Lawson, 1908).

Iwasaki *et al.* (1978) defined LPI as

$$\text{LPI} = \int_0^{20 \text{ m}} Fw(z) dz, \quad (1)$$

where

$$F = 1 - FS \quad \text{for } FS \leq 1, \quad (2a)$$

$$F = 0 \quad \text{for } FS > 1, \quad (2b)$$

and

$$w(z) = 10 - 0.5z, \quad (2c)$$

where z is the depth in meters. The weighting factor, $w(z)$, ranges from ten at the surface to zero at 20 m (Iwasaki *et al.*, 1978). $F = 0$ above the water table. LPI values can theoretically range from 0 to 100.

FS in this investigation was computed with the Seed–Idriss simplified procedure (Seed *et al.*, 1985) as modified for the CPT by Robertson and Wride (1998). This is the procedure recommended by Youd *et al.* (2001). This methodology is consistent with the calibration of LPI by Toprak and Holzer (2003), which relied on Robertson and Wride (1998) to compute FS . Toprak and Holzer (2003) evaluated the significance of LPI values by correlating LPI with surface manifestations of liquefaction. They observed that the median values of LPI were 5 and 12, respectively, in areas with sand boils and lateral spreads. Lower and upper quartiles, respectively, were 3 and 10 for sand boils and 5 and 17 for lateral spreads.

The advantage for hazard mapping of LPI over the simplified procedure is that it predicts the liquefaction hazard of the entire soil column at a specific location. The simplified procedure only predicts liquefaction potential of a soil element. By combining all of the factors of safety from a boring or sounding into a single value, LPI provides a spatially distributed parameter when multiple borings or soundings are conducted in a deposit.

The probability of surface manifestations of liquefaction for each surficial geologic unit was derived from complementary cumulative frequency distributions of LPI. Distributions were computed for a specific earthquake magnitude and water-table condition. By computing distributions for different PGA values, probability as a function of PGA can be estimated for each unit based on the frequency at $\text{LPI} \geq 5$. The procedure is illustrated in Figure 4. Figure 4a shows LPI distributions of young Holocene levee deposits (Qhly) in the Santa Clara Valley assuming a 5 m deep water table and an M 7.0 earthquake. Each distribution is based on a specific PGA and the same 25 CPT soundings conducted in Qhly. The probability of liquefaction at each PGA is the frequency value at $\text{LPI} \geq 5$ for each distribution. Figure 4b shows the liquefaction probability as a function of PGA for an M 7.0 earthquake. The probabilities were inferred from the fre-

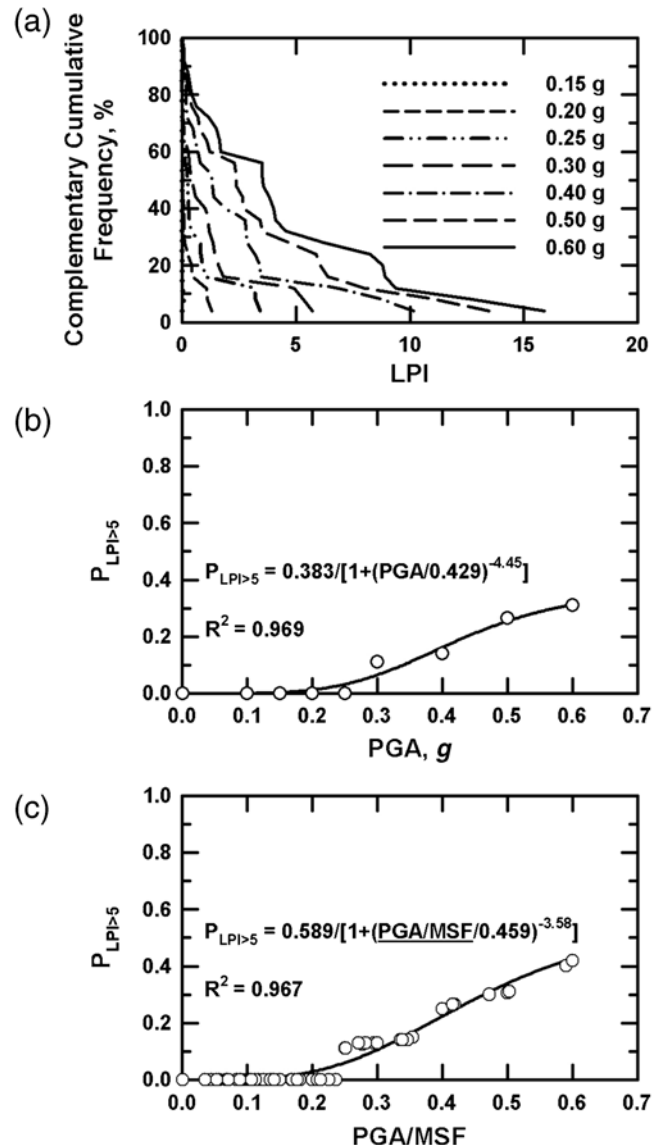


Figure 4. Liquefaction characteristics of surficial unit Qhly. (a) Complementary cumulative frequency distributions of LPI as a function of PGA for an M 7 earthquake and a water-table depth of 5 m; (b) probability of surface manifestations of liquefaction for an M 7 earthquake; and (c) liquefaction probability curve.

quency at $\text{LPI} \geq 5$ shown in Figure 4a. This methodology is the same as that used to map liquefaction hazard in the greater Oakland area (Holzer *et al.*, 2002; Holzer, Bennett, *et al.*, 2006; Holzer, Blair, *et al.*, 2006). Although the complementary cumulative frequency at $\text{LPI} \geq 5$ is interpreted here as the conditional probability of liquefaction at a randomly selected location within the area underlain by the geologic unit given an earthquake magnitude and PGA, it also can be interpreted as the percent area with surface manifestations of liquefaction (Holzer, Bennett, *et al.*, 2006).

Predicting the probability of liquefaction with spatially variable ground motions can be computationally simplified by curve fitting the relation between probability and PGA. Holzer, Blair, *et al.* (2006) recommended a three-parameter

logistic equation of the form shown in Figure 4b. Rix and Romero-Hudock (2007) generalized the probability relation to other earthquake magnitudes by scaling the seismic demand (PGA) by the magnitude scaling factor (MSF) from the simplified procedure (Fig. 4c). Data points in Figure 4c are probabilities from complementary cumulative frequency distributions computed for $5.5 \leq M \leq 8.0$ in 0.5 magnitude increments and $0 \leq \text{PGA} \leq 0.6g$ in 0.1 g increments. In the simplified procedure as described in Youd *et al.* (2001), $\text{MSF} = 10^{2.24/M-2.56}$. Holzer (2008) recommended that the relation between liquefaction probability and magnitude-scaled PGA for a surficial geologic unit be referred to as the liquefaction probability curve.

The Robertson and Wride (1998) simplified procedure does not require soil samples for liquefaction evaluation. This is a convenient advantage when dealing with large numbers of CPT soundings as was the situation in this investigation. The procedure uses the soil behavior index, I_C , to predict soil behavior. I_C values are determined with the normalized and dimensionless cone tip resistance and friction ratio using equation (3):

$$I_C = [(3.47 - \log Q)^2 + (1.22 + \log F)^2]^{0.5}, \quad (3)$$

where Q is the normalized tip resistance and F is the normalized friction ratio. Both are dimensionless.

For details of the normalization and nondimensionalization, the reader is referred to Robertson and Wride (1998). Values of I_C range from 1.64 or less for clean sands to values greater than 2.6 for silt mixtures and finer grained soils. Soils

with $I_C > 2.6$ are not considered to be susceptible to liquefaction. In the procedure as implemented by Robertson and Wride (1998) an apparent fines correction based on the I_C value is applied for soils with $1.64 < I_C < 2.6$.

On the basis of both the geologic setting inferred from CPT profiles in the Santa Clara Valley and from experience during hazard mapping of geologically similar deposits in greater Oakland (Holzer, Bennett, *et al.*, 2006), we were concerned that nonsusceptible fine-grained soils in the alluvial fan deposits soils with I_C values near but slightly less than 2.6 were being incorrectly classified as susceptible to liquefaction. This concern was greatest at sites with thick accumulations of fine-grained Holocene flood overbank deposits where I_C values varied around 2.6. Depth intervals with I_C values just slightly less than 2.6 at some of these sites contributed significantly to LPI values. To evaluate the capability of I_C to correctly classify the susceptibility of these fine-grained soils in the Santa Clara Valley, samples were collected adjacent to six soundings in geologic units Qhff, Qhf, and Qhl. Only a few sites were sampled because of challenges with permitting, but the selected sites were believed to be generally representative of surficial geologic units.

Soil samples collected at these sites indicated that the soil behavior index misclassified these fine-grained soils as susceptible to liquefaction. Geotechnical tests on these samples indicated the soil was not susceptible. This is illustrated in Figure 5, which compares the penetration profile for CPT SCC008 with geotechnical properties of soil samples from an adjacent 5 m deep boring. The sounding and adjacent boring were conducted in Qhff, the fine-grained alluvial

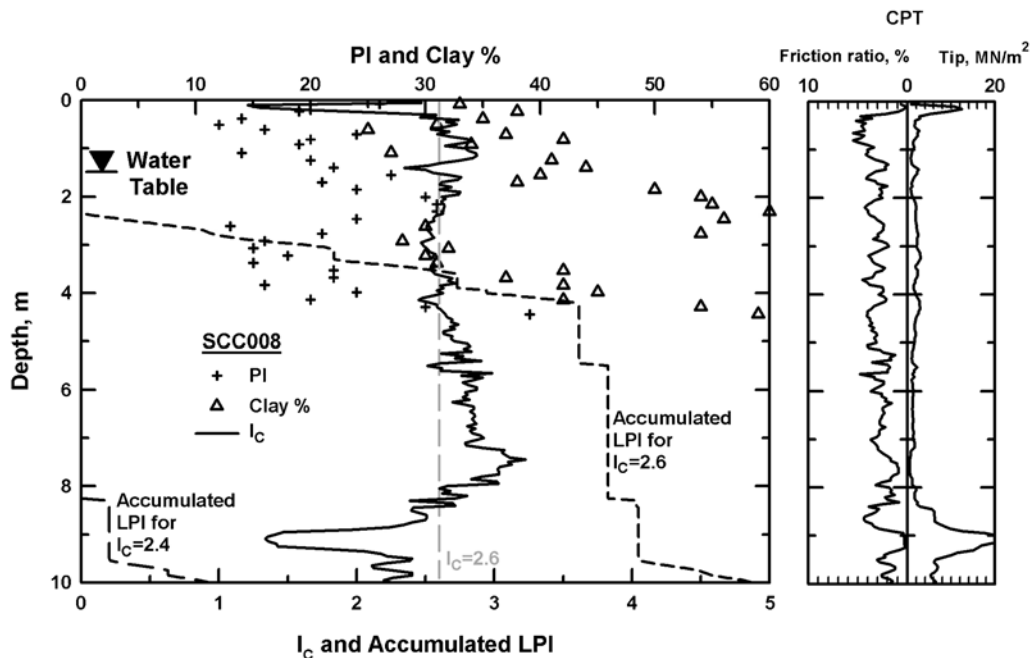


Figure 5. Comparison of penetration resistance at CPT SCC008 (right-hand panel) with soil properties of samples from adjacent boring (left-hand panel). Accumulated LPI curves show buildup of LPI with depth for I_C criteria of 2.4 and 2.6, a water-table depth of 1.5 m, and an M 7.5 earthquake with a PGA equal to 0.3g.

fan facies. The CPT SCC008 profile encountered an 8 m thick Holocene flood overbank deposit with an $I_C \approx 2.6$. Although the Robertson–Wride procedure predicts $FS < 1$ in the parts of the interval where I_C values are slightly less than 2.6, soil from the sampled depth interval, 0–5 m, is not susceptible to liquefaction according to criteria published by Bray and Sancio (2006) and Idriss and Boulanger (2006). The plasticity indices of the soil samples are generally greater than 12 and clay ($< 5 \mu\text{m}$) percentage ranges from 30% to 60%. The soil in the 8 m interval is a lean to fat clay (CL-CH in the Unified Soil Classification System).

The manner in which Robertson and Wride (1998) automated their procedure is a significant cause of the misclassification problem for Santa Clara Valley soils. Figure 6 shows the original Robertson (1990) soil behavior type classification chart. The chart divides soil behavior types into nine zones. Most of the F and Q values for the sampled intervals from SCC008 plot in zone 4 (see plus symbols in Fig. 6), which are nonsusceptible silt mixtures according to Robertson and Wride (1998). In order to automate the classification, Robertson and Wride (1998) approximated

the zone boundaries on the original chart with circles of constant I_C defined by equation (3). They approximated the boundary between zones 4 (silt mixtures) and 5 (sand mixtures) on the original chart by a circle with an $I_C = 2.6$. As is seen in Figure 6, equation (3) poorly approximates the boundary between zones 4 and 5 at normalized dimensionless friction ratios greater than 2, which is where most of the sampled depth intervals from SCC008 plot. Despite correctly plotting in zone 4, the I_C values for soils in the sampled interval are only slightly less than 2.6. Thus, most of the soil with $I_C < 2.6$ is misclassified by the automated procedure as susceptible sand mixtures rather than nonsusceptible silt mixtures.

To avoid (or at least decrease the incidence) of misclassifying nonsusceptible soils as susceptible in soundings without samples, we modified the automated Robertson–Wride procedure so that soils with $I_C > 2.4$ were classified as nonsusceptible. The effect of this modification on LPI in SCC008 is shown in Figure 5 by comparing the accumulation of LPI for both the modified ($I_C > 2.4$) and original criteria ($I_C > 2.6$) for nonsusceptibility. The interval in SCC008 that sampling indicates is nonsusceptible does not materially contribute to the accumulation of LPI with the $I_C > 2.4$ criterion. In fact, the accumulated LPI to a depth of 10 m for an M 7.5 earthquake and a PGA of 0.3g at SCC008 decreases from 4.9 to 0.9 when the I_C criterion for identifying nonsusceptible soil is reduced from 2.6 to 2.4 (Fig. 5).

The impact on computed liquefaction probabilities of using $I_C > 2.4$ rather than $I_C > 2.6$ as the criterion to identify nonsusceptible intervals is substantial and is illustrated by comparing Figure 7a and b. Figure 7a and b, respectively, show liquefaction probabilities for all of the major surficial geologic units if values of $I_C > 2.6$ and 2.4 are used as the criterion to identify soil intervals that are not susceptible to liquefaction. For the criterion $I_C > 2.6$, all of the geologic units have significant liquefaction probabilities, including the fine-grained Holocene alluvial fan unit, Qhff (Fig. 7a). Based on the criterion $I_C > 2.4$, probabilities of all units except Qhly decrease significantly. Probabilities for Qhly are only modestly reduced by introducing the new criterion (compare Fig. 7a and 7b). The modest effect in changing the susceptibility criterion and higher liquefaction probability of Qhly is consistent with the soil texture of Qhly along the lower reaches of Coyote Creek. Soundings in Qhly typically penetrated fluvial channel sands in which $I_C \approx 1.6$. Analyses of samples from adjacent borings confirm the CPT soil classification.

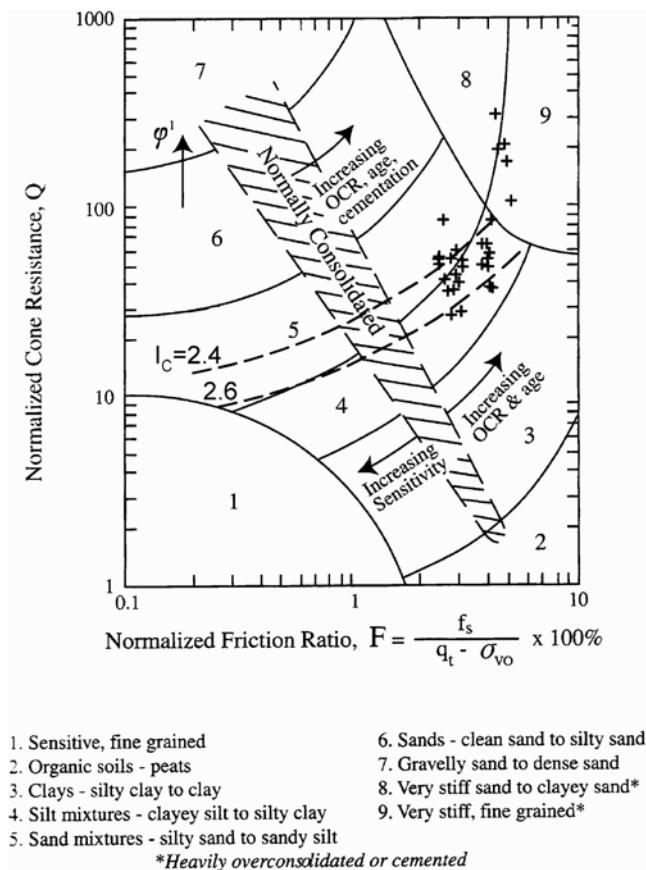


Figure 6. Soil behavior type at sampled depths (+ symbols) at CPT SCC008 predicted by the original Robertson (1990) soil behavior type classification chart. Soil samples were collected in an adjacent boring (see Fig. 5). Arc for $I_C = 2.6$ is the Robertson and Wride (1998) proposed approximation to the boundary between soil zones 4 and 5. Arc for $I_C = 2.4$ was used in current investigation to identify nonsusceptible soil.

Ground-Motion Prediction

PGA was estimated with the new ground-motion attenuation relation by Boore and Atkinson (2008). Their empirical relation predicts PGA as a function of earthquake magnitude and mechanism, fault type, closest distance to the surface projection of the fault plane (R_{JB}), and local site amplification. For the purpose here, both a strike-slip earthquake

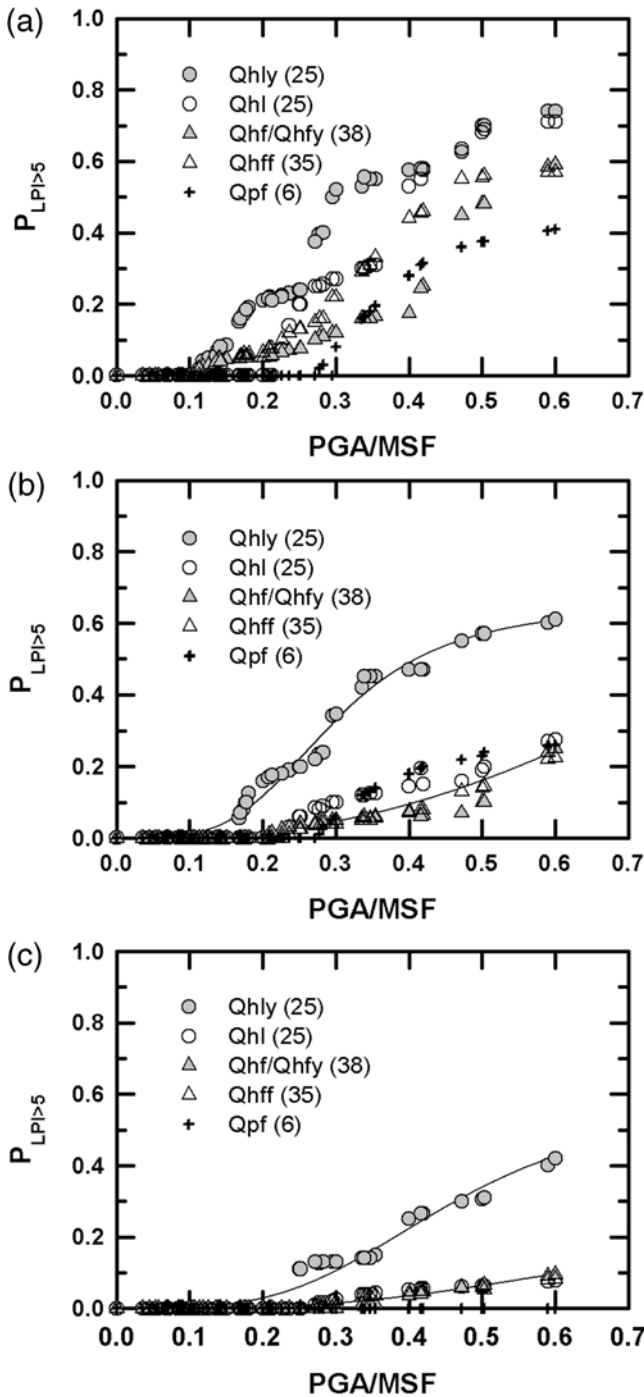


Figure 7. Liquefaction probability curves for alluvial fan deposits. (a) Water-table depth at 1.5 m and the $I_C \geq 2.6$ criterion used to identify nonsusceptible soil; (b) water-table depth at 1.5 m and the $I_C \geq 2.4$ criterion used to identify nonsusceptible soil; and (c) water-table depth at 5 m and the $I_C \geq 2.4$ criterion used to identify nonsusceptible soil. The number of CPT soundings in each surficial geologic unit is shown in parentheses. See Tables 1 and 2 for logistic regression equations.

mechanism and vertical fault type were assumed. Thus, spatial variations of PGA in the ground-motion model were caused only by variations of distance from the fault and local site conditions. As is common practice, Boore and Atkinson

(2008) use the time-averaged shear-wave velocity to 30 m (V_{S30}) to predict site amplification.

Examples of attenuation curves for M 6.7 and M 7.8 earthquakes, scenarios that were used here, are shown in Figure 8a. The attenuation curves are for a $V_{S30} = 235$ m/sec site condition, which is the average in the central part of the study area. The attenuation relations predict that PGA in the near field decays slowly with distance. In addition, differences of PGAs for M 6.7 and M 7.8 earthquakes in the near field are relatively small. This small difference is explained by soil nonlinearity in the Boore and Atkinson (2008) attenuation relation. This nonlinearity is illustrated in Figure 8b, which shows PGA predicted at $R_{JB} = 5$ km for different values of V_{S30} . The impact of nonlinearity in reducing PGA for values greater than 0.06 g increases as V_{S30} decreases from 300 m/sec.

The spatial variation of V_{S30} in the study area was approximated by subdividing the area underlain by Holocene alluvial fan deposits into two subareas based on the historically shallowest ground water table. Average values of V_{S30}

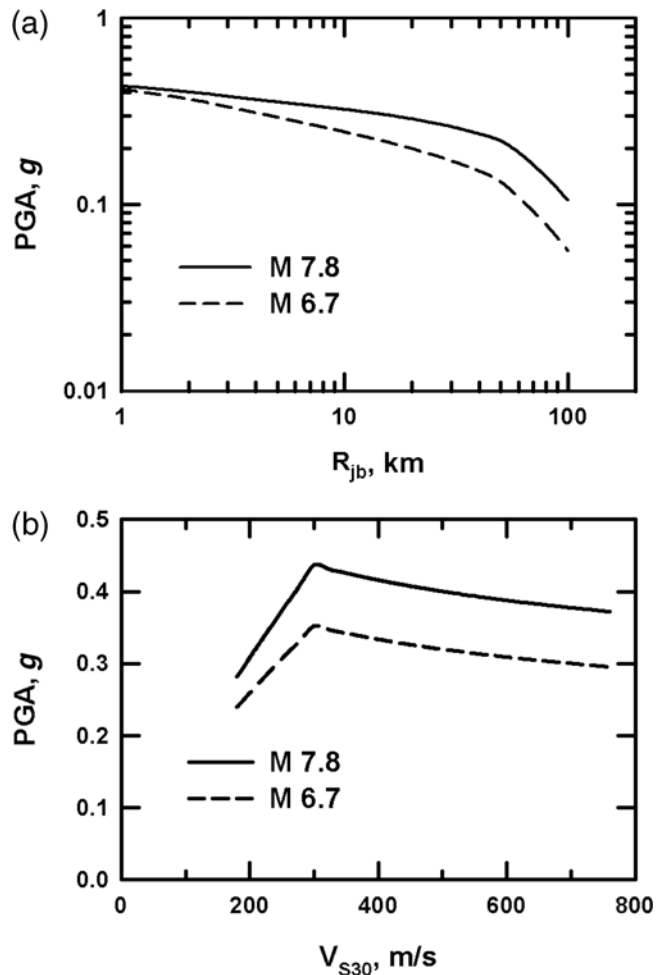


Figure 8. Median ground-motion predictions by Boore and Atkinson (2008). (a) PGA as a function of distance from fault (R_{JB}) for sites with $V_{S30} = 235$ m/sec and (b) PGA at 5 km as a function of V_{S30} .

were then computed for each subarea based on seismic CPT soundings. In the central subarea, the historically shallow water table was within 3 m of the land surface. In the surrounding subarea, the historically shallow water table was deeper than 3 m. Because most soundings were shallower than 30 m (average depth was 17.6 m), V_{S30} was estimated for each sounding by projecting the velocity measured at the bottom of the sounding to 30 m. In the central subarea, only soundings with a depth that exceeded 15 m were used. In the surrounding subarea, only soundings that exceeded 10 m were used.

Histograms of V_{S30} for each subarea are shown in Figure 9. Mean V_{S30} values in the central and outlying subareas are $235 (\pm 21)$ and $291 (\pm 62)$ m/sec, respectively. The greater dispersion of V_{S30} in the subarea surrounding the central subarea presumably is caused by the thinness of the Holocene alluvial fan deposits in the surrounding area and the greater variability of the underlying Pleistocene alluvial fan

deposits on V_{S30} . Pleistocene deposits around the valley margins have a broad range of ages and lithologies. Maps of V_{S30} indicate that values increase outward from the axis of the valley to the outlying subarea (not shown here).

Depth profiles of shear-wave velocity of Holocene and Pleistocene deposits are shown in Figure 10. Shear-wave travel times were measured with a single geophone at 2 m intervals and interval velocities were computed with the pseudointerval method. The profiles were created by assigning each interval velocity to the appropriate geologic deposit. Although velocities for each deposit exhibit considerable statistical dispersion, mean velocity values of the Holocene and

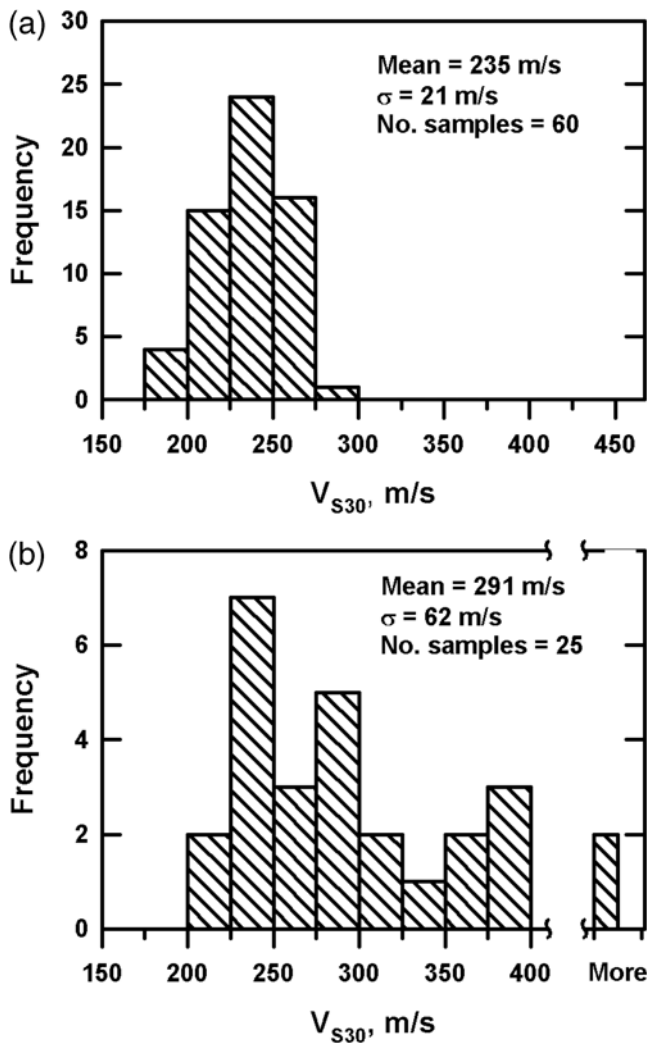


Figure 9. Histograms of V_{S30} inferred from seismic CPTs in the Santa Clara Valley for two subareas where the historically high water table was (a) less than 3 m deep and (b) more than 3 m deep.

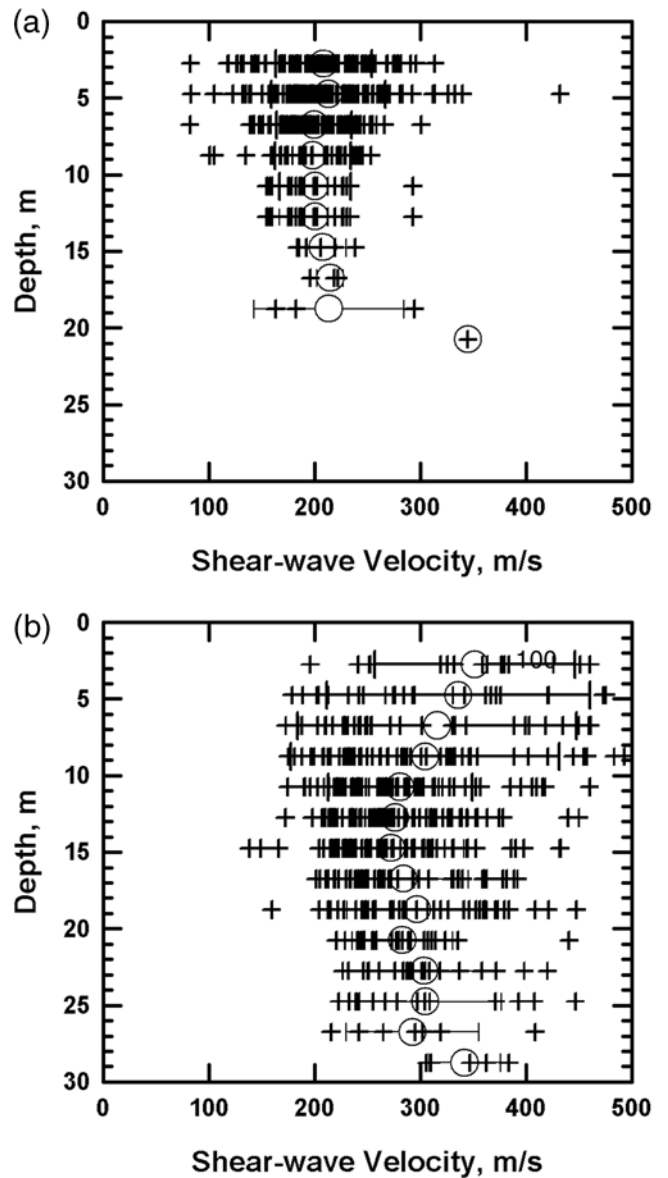


Figure 10. Profiles of 2 m interval shear-wave velocity for all seismic CPT soundings in the Santa Clara Valley for (a) Holocene and (b) Pleistocene alluvial fan deposits. An open circle denotes mean values and a horizontal bar denotes one standard deviation for each depth interval.

Pleistocene deposits, respectively, are significantly different, 207 (± 33) and 303 (± 77) m/sec. These velocities are slightly less than those reported by Holzer *et al.* (2005) for alluvial fan deposits in the greater Oakland area [224 (± 51) and 330 (± 84) m/sec], which is approximately 40 km northwest of the present study area.

Liquefaction Probability Curves

Computed probabilities of surface manifestations of liquefaction of the major surficial geologic units are shown in Figure 7b and c for two water-table depths, 1.5 and 5 m, respectively. These liquefaction probability curves were used to create the liquefaction hazard maps, which will be presented in the next section. The probabilities are based on the frequencies at $LPI \geq 5$ of the complementary cumulative frequency distributions for each surficial unit, using an $I_C \geq 2.4$ criterion to identify nonsusceptible soil. The number of CPT soundings in each surficial geologic unit is shown in parentheses in the legend (Fig. 7). The number of soundings per unit for the Holocene deposit ranged from 25 to 38.

Liquefaction probability curves for the major Holocene alluvial fan units in general are similar except for Qhly. Unit Qhly is significantly more liquefiable than the other Holocene alluvial fan units. Probabilities of surface manifestations of liquefaction of the other units in general are modest except for the 1.5 m deep water table and at high levels of ground motion ($PGA > 0.4 g$; Fig. 7b). The contrast in the probabilities between Qhly and the other units is even greater with the 5 m deep water table (Fig. 7c).

Because liquefaction probability curves for all of the Holocene fan units except for Qhly are approximately similar, curves for the non-Qhly units were averaged together to create a single curve. In addition to the obvious simplification for the map making process, there is a statistical argument to combine them. When the LPI-based liquefaction probability of a geologic unit is small, the number of samples, that is, CPT soundings, in the unit becomes an issue. For example, liquefaction probabilities of less than 0.05 in units with only 20 soundings are not statistically robust. By combining the units Qhl, Qhf/Qhfy, and Qhff into a single curve, the 98 soundings provide a more robust estimate of the liquefaction probability. The regression equations obtained by fitting a logistic curve to these data are shown in Table 1.

The reliability of predicted probabilities for the Pleistocene alluvial fan deposits is questionable. Although probabilities are zero for the 5 m deep water table (Fig. 7c), finite probabilities are predicted for the 1.5 m deep water ta-

ble (Fig. 7b). These probabilities are suspect on two bases, methodological and field experience. The probabilities were computed with six CPT soundings and only one sounding, SCC176, produced $LPI \geq 5$. The LPI was produced over the depth interval from 2 to 3 m that had a shear-wave velocity of 451 m/sec, which is anomalously high for liquefiable soil (Andrus *et al.*, 2004). In addition, many investigators have questioned the direct application of the field-based simplified procedure to pre-Holocene deposits because it may be overly conservative when applied to older deposits. The simplified procedure is based on case histories that include only Holocene deposits. These investigators (e.g., Leon *et al.*, 2006) have proposed using age corrections when applying the simplified procedure to older deposits. In addition to these methodological concerns, liquefaction of Pleistocene deposits in California has not been reported in historical earthquakes. Although liquefaction of these deposits cannot be precluded because liquefaction of deposits of Pleistocene age has been reported in earthquakes in the central and eastern United States (Obermeier *et al.*, 1990), probabilities were not assigned to areas underlain by these deposits.

In addition to using LPI to map the probability of surface manifestations of liquefaction, LPI also was used to map the probability of lateral spreading. Toprak and Holzer (2003) correlated the occurrence of lateral spreading with median LPI values of 12. This suggests that the complementary cumulative frequency at $LPI \geq 12$ can be used to predict the probability of lateral spreading. The probability curves for lateral spreads based on $LPI \geq 12$ are shown in Figure 11 for both 1.5 and 5 m water-table conditions. The logistic regression equations are shown in Table 2. The probabilities indicate that lateral spreading is likely only in areas underlain by Qhly. The reliability of lateral spread hazard maps based solely on LPI, however, remains to be demonstrated. Although a correlation between ground deformation and LPI is to be expected, lateral spreading also is influenced by factors not included in LPI, such as local static shear stress, continuity of liquefiable layers, and whether or not the soil is dilative or contractive. Nevertheless, we were curious about what an LPI-based lateral spread hazard map would look like and computed these probabilities in order to create these maps.

Liquefaction Hazard Maps

The final issue in the preparation of the liquefaction hazard maps was the depth to the water table. In our previous mapping of the greater Oakland area (Holzer, Bennett, *et al.*, 2006), the water table there was approximately stable, and we incorporated the observed water table in the LPI distributions. Both ground water and surface water in the Santa Clara Valley are managed by the Santa Clara Valley Water District. Thus, the water table is subject to anthropogenic influence. This and annual rainfall variations causes the water table to fluctuate significantly from periods of extended drought to periods of high rainfall. Accordingly, liquefaction hazard

Table 1
Logistic Regressions for Surficial Geologic Unit Qhly

Water-Table Depth (m)	Probability of Liquefaction	Probability of Lateral Spreading
1.5	$\frac{0.650}{1+[(PGA/MSF)/0.298]^{-3.78}}$	$\frac{0.388}{1+[(PGA/MSF)/0.419]^{-4.53}}$
5.0	$\frac{0.589}{1+[(PGA/MSF)/0.459]^{-3.58}}$	$\frac{0.262}{1+[(PGA/MSF)/0.577]^{-4.99}}$

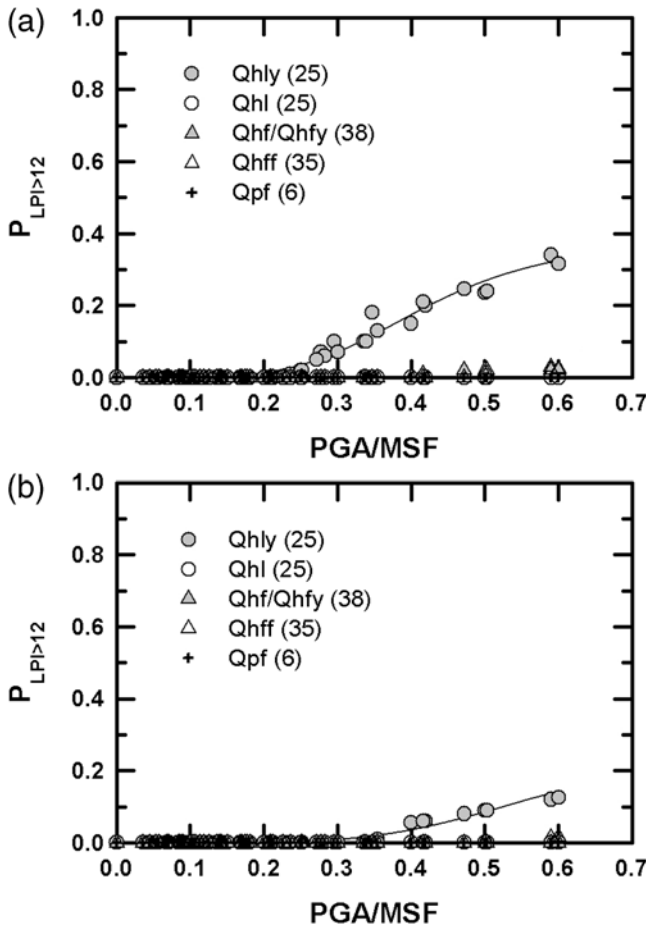


Figure 11. Probability of lateral spreading ($LPI > 12$) for water-table depths of (a) 1.5 m and (b) 5 m. The number of CPT soundings in the unit is shown in parentheses. See Tables 1 and 2 for logistic regression equations.

varies as the water table fluctuates with the hazard being lower during droughts than wet years. Defining the liquefaction hazard in the Santa Clara Valley is further challenged by the absence of detailed regional data showing depth to the water table. Unlike the investigation in greater Oakland, depths to water table could not be measured during the CPT field exploration because the Santa Clara Valley Water District requires grouting of sounding holes, which may remain open after the cone is withdrawn (Noce and Holzer, 2003).

To incorporate the effect of water-table depth on hazard, we relied on a map of the historically shallowest water table that was prepared by the California Geological Survey

(CGS). The map was prepared for regulatory seismic hazard mapping of the valley by CGS (see Data and Resources section). It was produced by using the shallowest water table observed in borings drilled over many decades. Although not a hydrologic snapshot of the water table, the map at least approximately portrays the shallowest water-table condition that is likely to be encountered over time within the study area. It therefore yields a conservative (i.e., highest liquefaction probability) hazard map. To computationally simplify the prediction of liquefaction probability in this investigation, the map of the historically shallowest water table was divided into two subareas separated by the 3 m (10 ft) contour of depth to the water table. This contour is shown in Figure 12. Within and outside this contour the liquefaction probability curves for water-table depths of 1.5 and 5 m, respectively, were applied. Consultant reports with irregular monitoring observations at leaking underground storage tanks in the study area, which are compiled at the Santa Clara Valley Local Oversight Program Public Record Document Search Web site (see Data and Resources section), permit comparison of current and historically shallowest water-table conditions. A selective review of these reports suggests that the current water table is near its historically shallow position at least in the central subarea. In addition, the reports suggest that the water table seasonally fluctuates only about 0.5 m in this area. Thus, even though generally conservative, the hazard maps of the central subarea approximate the current level of liquefaction hazard. Because the historically shallow water tables are substantially deeper than 5 m in most of the subarea outside of the 3 m contour, the hazard maps in this subarea presumably are very conservative.

Maps of liquefaction probability for three earthquake scenarios— M 7.8 San Andreas fault, M 6.7 Hayward fault, and M 6.9 Calaveras fault—with the 1.5 m deep water table in the central part of the study area are shown in Figure 12. These maps with the shallower water table approximately describe the most hazardous condition. Although probabilities can be computed with a high precision, probabilities on the hazard maps were grouped for mapping purposes into probability intervals of 0.1 and probabilities less than 0.05. All three earthquakes produce probabilities greater than 0.1 along parts of Coyote and Guadalupe Creeks. The highest probabilities, which range from 0.33 to 0.37, are in areas underlain by Qhly near the major creeks and are produced by the M 7.8 San Andreas fault earthquake. Probabilities range from 0.07 to 0.15 and from 0.10 to 0.13, respectively, in areas underlain by Qhly for the M 6.7 Hayward fault and the M 6.9 Calaveras fault earthquake scenarios. Probabilities elsewhere in the valley are less than 0.05 for all three earthquakes. The upper bound of the lower probability interval, 0.05, is somewhat arbitrary and reflects our low confidence in being able to distinguish between small liquefaction probabilities.

Probabilities were also computed for a water table that was assumed to be 5 m deep throughout the study area. The deeper water table yields a less conservative (i.e., lower

Table 2

Logistic Regressions for Surficial Geologic Units Qhf/Qhfy, Qhff, and Qhl

Water-Table Depth (m)	Probability of Liquefaction	Probability of Lateral Spreading
1.5	$\frac{1.83}{1+[(PGA/MSF)/1.25]^{-2.56}}$	0
5.0	$\frac{0.227}{1+[(PGA/MSF)/0.657]^{-3.43}}$	0

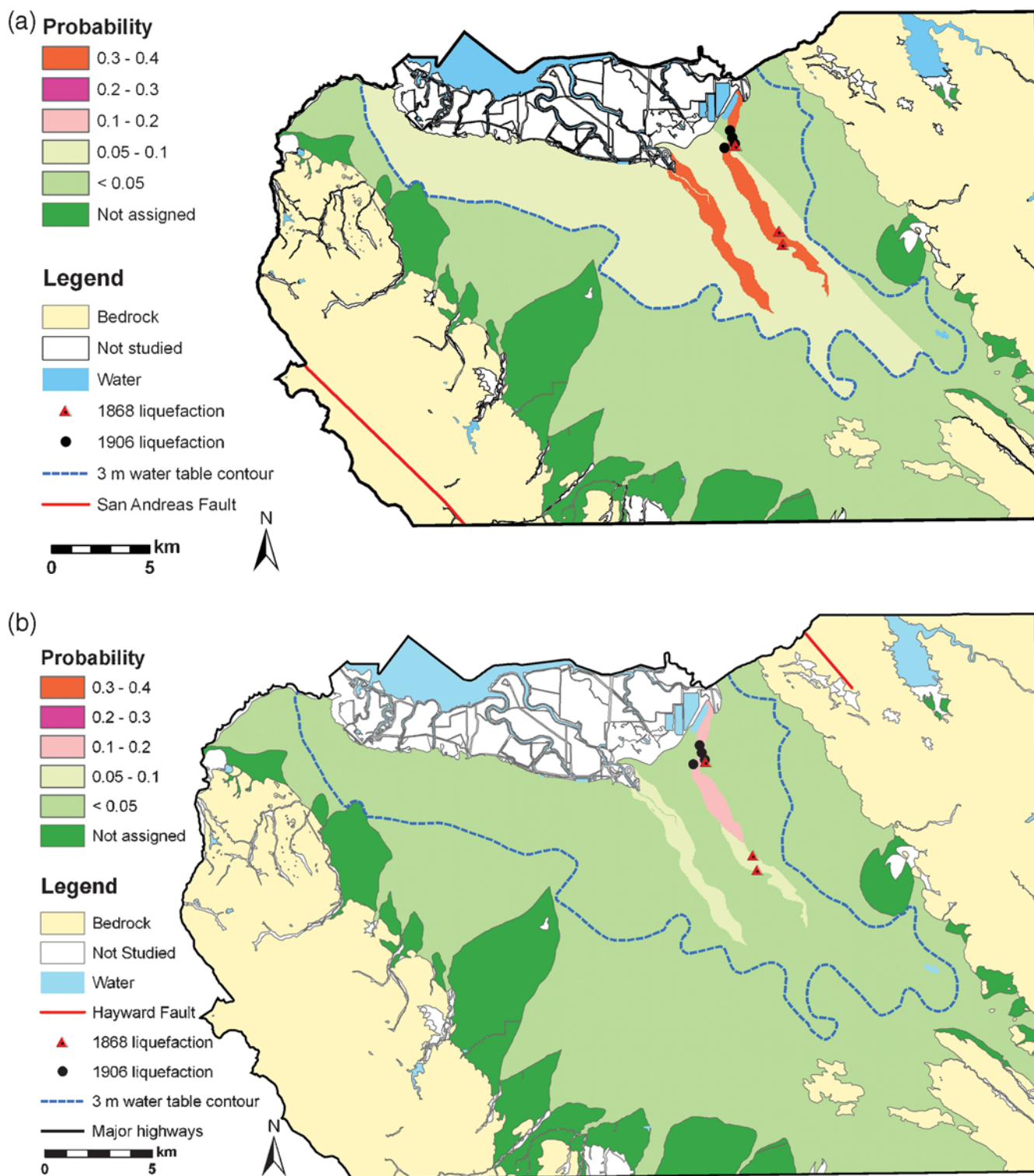


Figure 12. Liquefaction hazard maps for shallow water-table condition for (a) the M 7.8 San Andreas fault earthquake; (b) the M 6.7 earthquake on the Hayward fault; and (c) the M 6.9 earthquake on the Calaveras fault. *(Continued)*

hazard) map. With this water table, liquefaction probabilities decrease to less than 0.05 for all of the scenario earthquakes except the M 7.8 San Andreas fault earthquake. Probabilities range from 0.10 to 0.14 in areas underlain by Qhly along the creeks for the M 7.8 earthquake (Fig. 13).

Figure 14 illustrates a lateral spread hazard map based on LPI. The probability of lateral spreading is based on the $LPI \geq 12$ criterion (Fig. 11). The probability of lateral spreading is locally greater than 0.05 for only the M 7.8 San Andreas fault earthquake scenario with the shallow 1.5 m deep

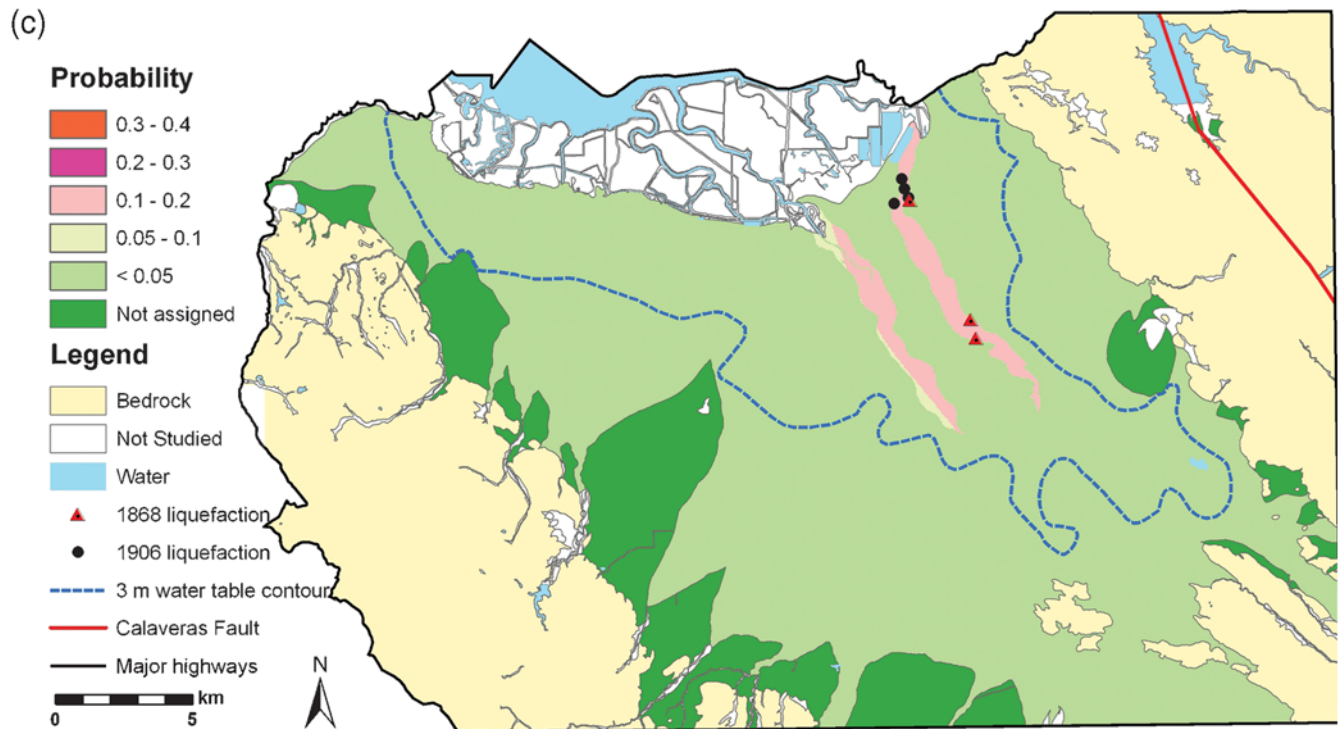


Figure 12. Continued.

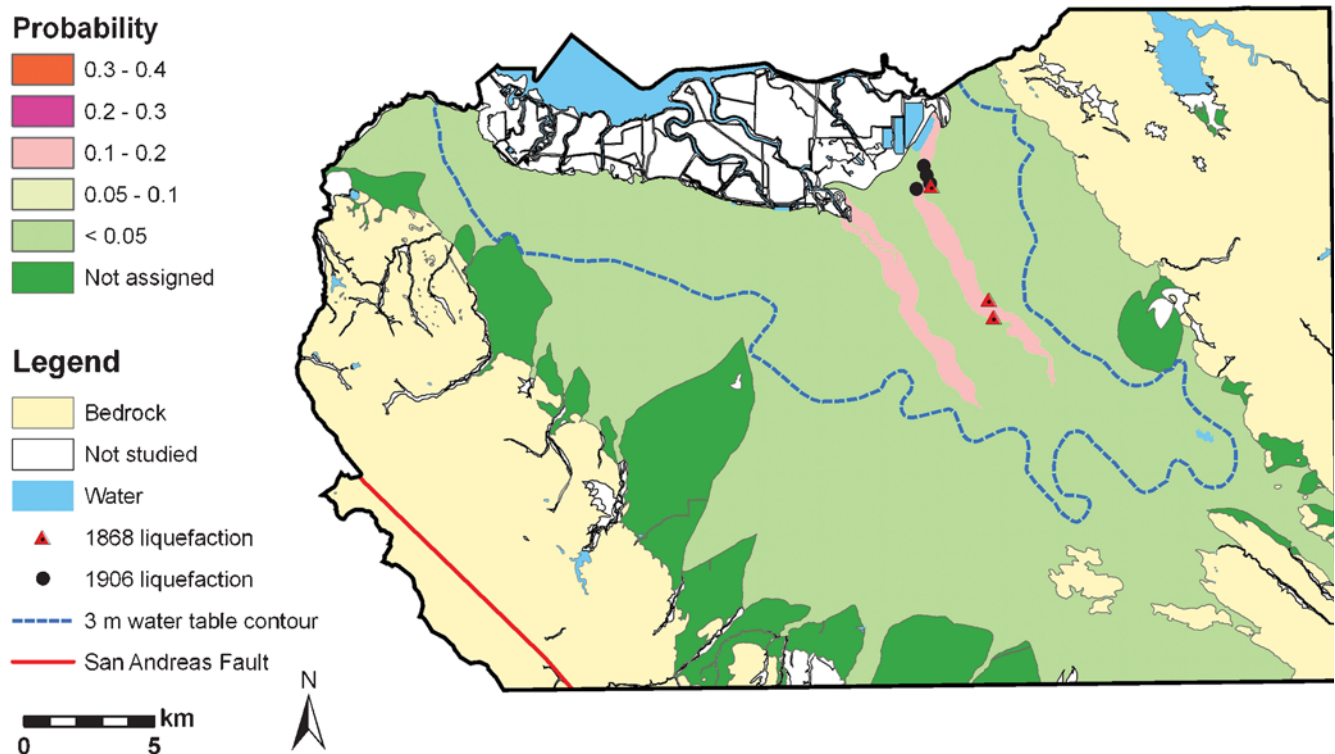


Figure 13. Liquefaction hazard map for 5 m deep water table for the M 7.8 earthquake on the San Andreas fault.

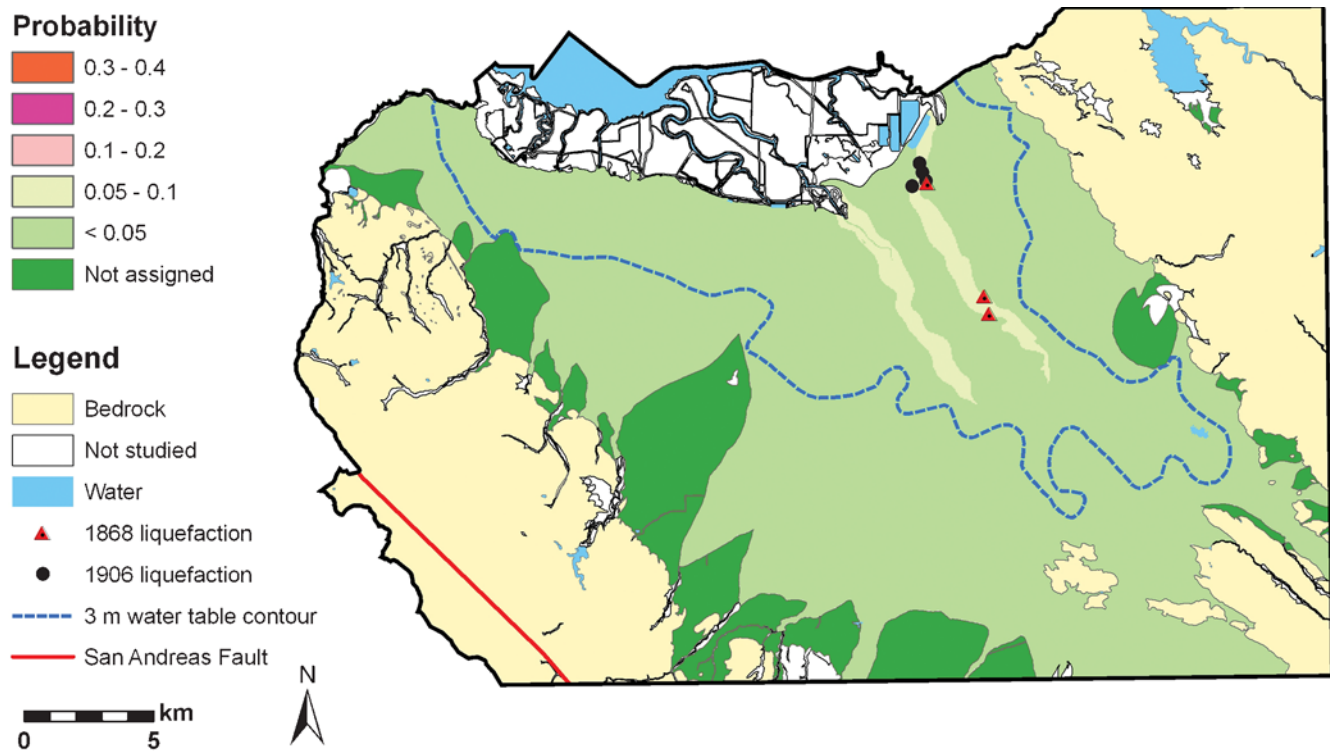


Figure 14. Lateral spread hazard map for shallow water-table condition for the M 7.8 earthquake on the San Andreas fault.

water table (Fig. 14). Probabilities range from 0.06 to 0.09 in areas underlain by Qhly along the creeks for this earthquake and the shallow water table. Probabilities of lateral spreading are less than 0.01 for all of the other earthquake scenarios, as well as the M 7.8 San Andreas fault earthquake scenario, when the water table is assumed to be 5 m deep.

Discussion

Although a rigorous test of the mapped predictions in the study area with observations of liquefaction in historical earthquakes is not possible, a qualitative comparison with observations during the 1868 Hayward fault and 1906 San Francisco earthquakes is possible. In addition, the absence of liquefaction during the 1989 M 6.9 Loma Prieta earthquake can be used to evaluate the methodology.

Both Lawson (1908) and Youd and Hoose (1978) reported extensive ground failure along Coyote Creek that indicates liquefaction was widespread in both the 1868 and 1906 earthquakes. Descriptions include sand boils, settlements, and lateral spreading. Some of the descriptions are confirmed with photographs (e.g., Fig. 3), which leaves little doubt about the nature of the mechanism of ground failure. Although Lawson (1908) did not map these occurrences, descriptions of landmarks and references to property ownership where effects were observed permit fairly accurate locations of many observations (Youd and Hoose, 1978). In addition to these descriptions, Youd and Hoose (1978) added accounts from newspapers. We reviewed these locations and plotted

them on the geologic map (Fig. 2) and the liquefaction hazard maps. All of the liquefaction reports are located in the area underlain by Qhly, the unit with the highest liquefaction probability. No liquefaction appears to be associated with the other Holocene units. This is consistent with the observation by Youd and Hoose (1978, p. 23) that “no significant failures were reported on late Pleistocene and most Holocene alluvial fan deposits at points well removed from active stream channels.”

Although it would be helpful for assessing the reliability of the hazard maps if the percent of the area underlain by Qhly that liquefied in 1906 could be estimated, descriptions compiled by Lawson (1908) and Youd and Hoose (1978) do not permit this assessment. Nevertheless, their descriptions clearly indicate that liquefaction was extensive along and near Coyote Creek. These descriptions are generally consistent with the maps in Figures 12 and 13. For the shallower water-table condition, the percentage of area underlain by Qhly that is predicted to exhibit surface manifestations of liquefaction in 1868 and 1906, respectively, ranged from 7% to 15% and from 33% to 37%. For the deeper water table, only the 1906 earthquake yielded areal estimates greater than 5, ranging from 10% to 14%. Depths to the water table are unknown during both of these historical earthquakes, although the water table was probably shallower during the 1906 earthquake than during the 1868 earthquake. The former earthquake occurred in April near the end of the rainy season, and the latter earthquake occurred in October near the end of dry season.

Liquefaction probabilities (not shown) were also computed for the 1989 M 6.9 Loma Prieta earthquake, which ruptured a segment of the San Andreas fault south of the study area. As noted previously, surface effects of liquefaction were not observed in 1989 (Holzer, 1998). Computed liquefaction probabilities in Qhly for the 1989 earthquake were less than 0.02 for the 5 m deep water-table condition. The Loma Prieta earthquake occurred on 17 October 1989 near the end of the dry season when water tables typically are deepest.

The liquefaction hazard maps for the northern Santa Clara Valley highlight the need for meaningful observations of depth to the water table. Without such information, the accuracy of the hazard map is compromised. This issue of water-table depth is further complicated in the Santa Clara Valley because of the conjunctive management of ground and surface water. This causes the hazard to vary secularly depending on climatic conditions. The impact of the position of the water table on liquefaction probability is illustrated in Figure 15, which shows liquefaction probability curves for Qhly for different water-table depths. Probabilities decay approximately monotonically to zero when the water table reaches a depth of ~ 9 m. This corresponds to the average thickness of Qhly in the central subarea, which implies that the saturated thickness of Qhly is critical in determining the liquefaction hazard.

The adoption in this investigation of $I_C > 2.4$ as the criterion to identify soils that are not susceptible to liquefaction significantly reduced the probabilities of liquefaction for all of the surficial geologic units but Qhly. Although we are not prepared to recommend a basic change in the Robertson and Wride (1998) procedure to incorporate this criterion, three considerations justified its adoption in the present investigation. First, sampled nonsusceptible soils in the Santa Clara

Valley plot in zone 4 on the Robertson (1990) original soil behavior type chart. This zone includes nonsusceptible silt mixtures. An I_C equal to 2.4 rather than 2.6 better approximates the soil behavior type boundary between zones 4 and 5, where $F > 2$, and thereby properly classifies these soils. Second, the modified criterion is consistent with the synthesis of CPT observations at 78 sites in Japan, where liquefaction is known either to have or not to have occurred during earthquakes (Suzuki *et al.*, 2003). They reported no liquefaction where $I_C > 2.4$. And third, the probability curves based on an $I_C > 2.4$ criterion reasonably predict the observed patterns of liquefaction in this investigation. If the original $I_C > 2.6$ criterion had been applied, significant liquefaction would have been predicted in the alluvial fan areas where no historical liquefaction has been reported.

Liquefaction probabilities predicted for Qpf, although not statistically robust because of the small number of soundings, highlight an ongoing issue with the application of the simplified procedure to soils that predate the Holocene epoch. As previously noted, the straightforward application of the procedure to these older soils has been challenged by multiple investigators because it appears to underestimate their liquefaction resistance. This shortcoming and the absence of reports of liquefaction associated with Pleistocene deposits in historical California earthquakes prompted us not to assign probabilities predicted with the simplified procedure to areas underlain by these older deposits. Liquefaction of Pleistocene deposits, however, has been reported in several non-California earthquakes in the United States. It was observed in late Pleistocene valley train deposits during the 1811–1812 New Madrid, Missouri, earthquakes and in Pleistocene beach ridges during the 1886 Charleston, South Carolina, earthquake (Obermeier *et al.*, 1990). Improving the reliability of the simplified procedure for predicting the liquefaction potential of Pleistocene deposits is an important research need for liquefaction hazard mapping.

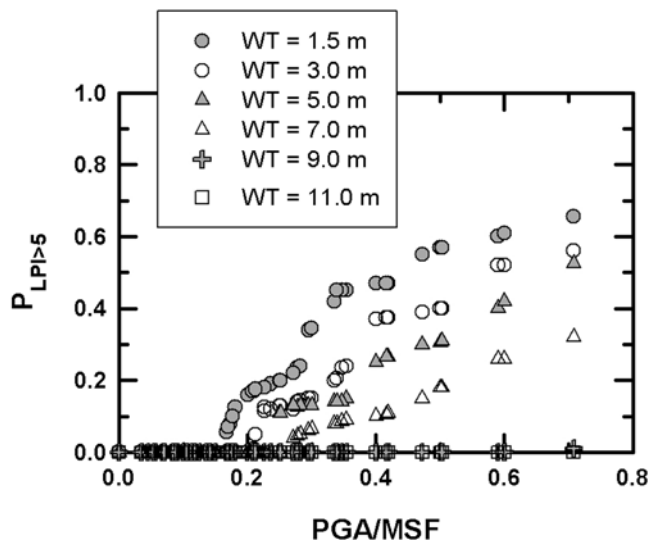


Figure 15. Dependency of liquefaction probability curves for Qhly on depth to water table (WT).

Data and Resources

CPT data collected by the USGS are available at the Earthquake Program Web site (<http://earthquake.usgs.gov/regional/nca/cpt/index.php>, last accessed October 2008). Data used to prepare California Geological Survey Seismic Hazard Zone Maps can be downloaded by registering at their Web site. The map of historical high water level is not available for downloading but the data used to construct it are available (<http://www.consrv.ca.gov/cgs/shzp/>, last accessed September 2008). Consulting reports at leaking underground storage tanks study sites are available at the Santa Clara Valley Local Oversight Program Public Record Document Search by selecting “city” in the scroll down menu and clicking on “search” (<http://lustop.sccgov.org>, last accessed August 2008).

Acknowledgments

Reviews by Ronald D. Andrus and John C. Tinsley III of an early draft of this manuscript are appreciated. The authors are also indebted to the anonymous journal reviews for their insightful comments. We also thank George Cook for alerting us to the consulting reports with repeated water-table observations. Coyn Criley performed the soil index tests on samples from SCC008.

References

- Andrus, R. D., K. H. Stokoe, and C. H. Juang (2004). Guide for shear-wave-based liquefaction potential evaluation, *Earthq. Spectra* **20**, 285–308.
- Boore, D. M., and G. M. Atkinson (2008). Ground-motion prediction equations for the average horizontal component of PGA, PGV, and 5%-damped PSA at spectral periods between 0.01 s and 10.0 s, *Earthq. Spectra* **24**, 99–138.
- Bray, J. D., and R. B. Sancio (2006). Assessment of the liquefaction susceptibility of fine-grained soils, *J. Geotech. Geoenviron. Eng. ASCE* **132**, 1165–1177.
- Building Seismic Safety Council (BSSC) (2001). 2000 Edition NEHRP recommended provisions for seismic regulations for new buildings and other structures, FEMA 368, Part 1 (provisions), Federal Emergency Management Agency, 374 pp.
- California Geological Survey (CGS) (2004). Recommended criteria for delineating seismic hazard zones in California, *Calif. Div. Mines Geol. Spec. Publ. 118*, 12 pp.
- Cornell, C. A. (1968). Engineering seismic risk analysis, *Bull. Seismol. Soc. Am.* **58**, 1583–1606.
- Holzer, T. L. (Editor) (1998). The Loma Prieta, California, earthquake of October 17, 1989—Liquefaction, *U.S. Geol. Surv. Profess. Pap. 1551-B*, 314 pp.
- Holzer, T. L. (2008). Probabilistic liquefaction hazard mapping, in *Proc. 4th Geotechnical Earthquake Engineering and Soil Dynamics Conference*, Sacramento, California, 18–22 May 2008, ASCE Geotech. Spec. Publ. 181, 1–32.
- Holzer, T. L., M. J. Bennett, T. E. Noce, A. C. Padovani, and J. C. Tinsley III (2002). Liquefaction hazard and shaking amplification maps of Alameda, Berkeley, Emeryville, Oakland, and Piedmont: a digital database, *U.S. Geol. Surv. Open-File Rept. 02-296*: available at <http://pubs.usgs.gov/of/2002/02-296>, last accessed January 2008.
- Holzer, T. L., M. J. Bennett, T. E. Noce, and J. C. Tinsley III (2005). Shear-wave velocity of surficial geologic sediments in Northern California, statistical distributions and depth dependence, *Earthq. Spectra* **21**, 161–177.
- Holzer, T. L., M. J. Bennett, T. E. Noce, A. C. Padovani, and J. C. Tinsley III (2006). Liquefaction hazard mapping with LPI in the greater Oakland, California, area, *Earthq. Spectra* **22**, 693–708.
- Holzer, T. L., J. L. Blair, T. E. Noce, and M. J. Bennett (2006). Predicted liquefaction of East Bay fills during a repeat of the 1906 San Francisco earthquake, *Earthq. Spectra* **22**, S261–S278.
- Idriss, I. M., and R. W. Boulanger (2006). Semi-empirical procedures for evaluating liquefaction potential during earthquakes, *Soil Dyn. Earthq. Eng.* **26**, 115–130.
- Iwasaki, T., D. Tatsuoka, K.-i. Tokida, and S. Yasuda (1978). A practical method for assessing soil liquefaction potential based on case studies at various sites in Japan, in *Proc. 2nd Int. Conf. on Microzonation*, San Francisco, 885–896.
- Lawson, A. C. (Editor) (1908). The California earthquake of April 18, 1906, Report of the State Earthquake Investigation Commission, Carnegie Institution Washington Publication **87**, 451 pp.
- Leon, E., S. L. Gassman, and P. Talwani (2006). Accounting for soil aging when assessing liquefaction potential, *J. Geotech. Geoenviron. Eng. ASCE* **132**, 363–377.
- McGuire, R. K. (2004). Seismic hazard and risk analysis, Earthquake Engineering Research Institute Monograph **10**, 221 pp.
- Noce, T. E., and T. L. Holzer (2003). CPT-hole closure, *Ground Water Monit. Remediat.* **23**, 93–96.
- Obermeier, S. F., R. Jacobson, J. Smoot, R. E. Weems, G. S. Gohn, J. E. Monroe, and D. S. Powars (1990). Earthquake-induced liquefaction features in the coastal setting of South Carolina and in the fluvial setting of the New Madrid seismic zone, *U.S. Geol. Surv. Profess. Pap. 1504*, 44 pp.
- Rix, G. J., and S. Romero-Hudock (2007). Liquefaction potential mapping in Memphis and Shelby County, Tennessee, unpublished Rept. to the U.S. Geol. Surv., Denver, Colorado, 27 pp: available at http://earthquake.usgs.gov/regional/ceus/products/download/Memphis_LPI.pdf, last accessed January 2008.
- Robertson, P. K. (1990). Soil classification using the CPT, *Can. Geotech. J.* **27**, 151–158.
- Robertson, P. K., and C. E. (Fear) Wride (1998). Evaluating cyclic liquefaction potential using the cone penetration test, *Can. Geotech. J.* **35**, 442–459.
- Seed, H. B., K. Tokimatsu, L. F. Harder, and R. M. Chung (1985). Influence of SPT procedures in soil liquefaction resistance evaluations, *J. Geotech. Eng. ASCE* **111**, 1425–1445.
- Suzuki, Y., K. Tokimatsu, and K. Koyamada (2003). Correlation between soil liquefaction during earthquakes and CPT data, *J. Struct. Constr. Eng.* **571**, 95–102.
- Toprak, S., and T. L. Holzer (2003). Liquefaction potential index: field assessment, *J. Geotech. Geoenviron. Eng. ASCE* **129**, 315–322.
- Wentworth, C. M., and J. C. Tinsley (2005). Tectonic subsidence and cyclic Quaternary deposition controlled by climate variation, Santa Clara Valley, California (abstract), *Geol. Soc. Am. Abstr. Programs* **37**, no. 4, 59.
- Witter, R. C., K. L. Knudsen, J. M. Sowers, C. M. Wentworth, R. D. Koehler, and C. E. Randolph (2006). Maps of Quaternary deposits and liquefaction susceptibility in the central San Francisco Bay region, California, *U.S. Geol. Surv. Open-File Rept. 06-1037*: available at http://pubs.usgs.gov/of/2006/1037/of06-1037_1c.pdf, last accessed January 2008.
- Working Group on California Earthquake Probabilities (WGCEP) (2003). Earthquake probabilities in the San Francisco Bay region 2002–2032, *U.S. Geol. Surv. Open-File Rept. 03-214*: available at <http://pubs.usgs.gov/of/2003/of03-214/>, last accessed January 2008.
- Youd, T. L., and S. N. Hoose (1978). Historic ground failures in Northern California triggered by earthquakes, *U.S. Geol. Surv. Profess. Pap.* **993**, 177 pp.
- Youd, T. L., I. M. Idriss, R. D. Andrus, I. Arango, G. Castro, J. T. Christian, R. Dobry, W. D. L. Finn, L. F. Harder Jr., M. E. Hynes, K. Ishihara, J. P. Koester, S. S. C. Liao, W. F. Marcuson III, G. R. Martin, J. K. Mitchell, Y. Moriwaki, M. S. Power, P. K. Robertson, R. B. Seed, and K. H. Stokoe II (2001). Liquefaction resistance of soils: summary report from the 1996 NCEER and 1998 NCEER/NSF workshops on evaluation of liquefaction resistance of soils, *J. Geotech. Geoenviron. Eng. ASCE* **127**, 817–833.

U.S. Geological Survey
345 Middlefield Road
Menlo Park, California 94025
tholzer@usgs.gov
tnoce@usgs.gov
mjbennett@usgs.gov